Large Time Step Roe scheme for a common 1D two-fluid model

Marin Prebeg[a], Tore Flåtten[b], Bernhard Müller[a]

[a] *Department of Energy and Process Engineering, Norwegian University of Science and Technology, Kolbjørn Hejes vei 2, Trondheim, Norway*
[b] *SINTEF Materials and Chemistry, Oil and Gas Process Technology, S. P. Andersens veg 15 B, Trondheim, Norway*

Abstract

We present the Large Time Step (LTS) extension of the Roe scheme and apply it to a standard two-fluid model. Herein, LTS denotes a class of explicit methods that are not limited by the CFL (Courant–Friedrichs–Lewy) condition, allowing us to use very large time steps compared to standard explicit methods. The LTS method was originally developed in the nineteen eighties (LeVeque, 1985), where the Godunov scheme was extended to the LTS Godunov scheme. In the present work, the relaxation of the CFL condition is achieved by increasing the domain of dependence. This might lead to difficulties when it comes to boundary and source terms treatment. We address and discuss these difficulties and propose different ways to treat them. For a shock tube test case, where there are neither source terms nor difficulties associated with the boundaries, the method increases both accuracy and efficiency. For a water faucet test case that includes a source term, the method increases the efficiency, while the accuracy strongly depends on the appropriate treatment of boundary conditions and source terms.

Keywords: Large Time Step method, Roe scheme, Two-fluid model, Boundary treatment, Source term

1. Introduction

In this paper, we are interested in the numerical simulation of one dimensional two-phase flow. To that end, we use a one dimensional, equal-pressure two-fluid model studied by many authors [1, 2, 3, 4, 5, 6]. This and other similar models are in widespread use for the simulation of two-phase flow, and they have been used successfully in many applications by the oil & gas [7, 8] and nuclear industry [9]. In practical applications one usually has to make a compromise between accuracy and efficiency. The balance between these requirements is, among other things, strongly affected by the numerical time integration method, where the main division is made between explicit and implicit time integration methods. As is well known, explicit methods are associated with higher accuracy and simpler implementation, but their efficiency and stability are limited by the CFL (Courant–Friedrichs–Lewy) condition. Implicit methods are not limited by the CFL condition and may be very efficient, but they are associated with a number of different difficulties, most important being the excessive diffusion and difficult parallelization. In this paper we study a class of explicit methods that are not limited by the CFL condition, thereby allowing us to use time steps much larger than usually associated with explicit methods. Such methods are knows as the Large Time Step (LTS) methods and they have been first introduced in the nineteen eighties by LeVeque [10, 11, 12]. Therein, the Godunov scheme was extended to the LTS Godunov scheme and applied to scalar conservation laws and the Euler equations.

In his work, LeVeque treats each discontinuity as a wave and allows waves from each Riemann problem to travel more than one cell during a single time step, allowing for interaction between the waves. These interactions are assumed to be linear, i.e. the waves are passing through each other without change in speed or strength [12]. From the way LeVeque's LTS method is defined, it uses a Lagrangian point of view by tracking where the characteristics are going. Through the years, these ideas have been recognized and used by many authors. Here, we address the most recent contributions, without attempting to provide a complete and comprehensive overview.

Murillo, Morales-Hernández and co-workers [13, 14, 15, 16] applied the LTS Roe scheme to the one and two dimensional shallow water equations and focused on the treatment of source terms and boundary conditions. Xu et al. [17] applied the LTS Godunov scheme to the shallow water equations. Qian and Lee [18] applied the LTS Godunov scheme to the three dimensional Euler equations by using a dimensional splitting approach. Tang et al. [19] applied the LTS Godunov scheme to high speed combustion waves. Makwana and Chatterjee [20] applied the LTS Godunov scheme to the Maxwell's equations, and Lindqvist and Lund [21] applied the LTS Roe scheme to two-phase flow and focused on accuracy and computational efficiency. Lindqvist et al. [22] also studied more theoretical properties of the LTS methods and how they fit into the TVD setting. Therein, the LTS method of LeVeque is defined in the numerical viscosity and flux difference splitting framework, a perspective more coinciding with the Eulerian point of view. It is shown that these formulations are mathematically equivalent to the original formulation by LeVeque [12].

Herein, we use the LTS method of LeVeque in the form presented by Lindqvist et al. [22] and apply it to the one dimensional non-conservative two-fluid model. In [22], the relaxation of the CFL condition is achieved by extending the domain of dependence. This leads to difficulties when it comes to the treatment of boundary conditions and source terms. These issues are the central topic of this paper. For the homogeneous system, the LTS Roe scheme shows promising results when applied to test cases where no complex wave interactions occur at the boundaries, as will be illustrated by the numerical example of the shock tube. However, "interesting" boundaries and/or source terms require special treatment. In the present paper we will illustrate difficulties related to the boundary conditions and source terms as separate challenges, using the classical water faucet test case as an example. First, we will discuss the definition of the boundary conditions in the LTS Roe scheme. Namely, the presence of source terms may lead to a distinct pattern of numerical errors being generated in the vicinity of the boundary. We will show how boundary conditions can be modified to reduce these errors and improve the accuracy of the solution. Second, the presence of source terms in the LTS Roe scheme may lead to numerical errors being generated elsewhere in the domain as well. We will discuss how these errors are generated and show that the most simple, straightforward treatment of source terms is not well suited for the LTS method. To resolve this, we will discretize the source term by formulating a slight modification to the approach presented by Murillo and García-Navarro [23]. The separate treatment of the difficulties related to the boundary conditions and source terms will be justified in sections 4 and 5, where we will show that the numerical errors being generated in the vicinity of the boundary and elsewhere in the domain are caused by distinct but related mechanisms.

This paper is structured as follows: in section 2, we present the two-fluid model we use. In section 3, we present the numerical method and outline the standard Roe and LTS Roe schemes. Sections 4 and 5 discuss boundary and source term treatments, respectively, with corresponding numerical investigations. Section 6 discusses accuracy and computational performance, and section 7 closes with conclusions.

2. Mathematical model

We are considering a one dimensional isentropic equal-pressure two-fluid model [1, 2, 3, 4, 5, 6] without energy equation, where we solve separate evolution equations for mass and momentum of two fluids:

$$\partial_t(\alpha_g\rho_g) + \partial_x(\alpha_g\rho_g v_g) = 0, \tag{2.1}$$

$$\partial_t(\alpha_l\rho_l) + \partial_x(\alpha_l\rho_l v_l) = 0, \tag{2.2}$$

$$\partial_t(\alpha_g\rho_g v_g) + \partial_x(\rho_g\alpha_g v_g^2 + (p - p^i)\alpha_g) + \alpha_g\partial_x p^i = Q_g, \tag{2.3}$$

$$\partial_t(\alpha_l\rho_l v_l) + \partial_x(\rho_l\alpha_l v_l^2 + (p - p^i)\alpha_l) + \alpha_l\partial_x p^i = Q_l, \tag{2.4}$$

where ρ, α, v, Q are the density, volume fraction, velocity and the source term with corresponding phase indices g, l for the gas and liquid phase, respectively. The pressure p denotes a common pressure of both phases, while the pressure p^i denotes the pressure at the interface between gas and liquid.

In this basic model, several physical effects that would be present for a number of engineering applications have been neglected. For numerical studies, this practice has been followed by many authors [1, 2, 3, 4, 5, 6] and a thorough discussion of its justification can be found in the book of Städtke [24].

In this respect, we would like to emphasize that a number of practical applications would require viscous terms [25], i.e. terms involving second-order spatial derivatives, to be naturally incorporated into our framework. Such terms would typically render the model parabolic, and would be physically important for problems involving for instance thermal conduction or wax deposition. As demonstrated in [22], our numerical Large Time Step framework naturally includes numerical diffusion. This was exploited by Solberg [26] who proposed a concrete extension of the LTS framework to systems containing viscous terms.

2.1. Quasilinear form

The Eqs. (2.1)–(2.4) can be written in a quasilinear form as:

$$\partial_t\mathbf{U} + \mathbf{A}(\mathbf{U})\partial_x\mathbf{U} = \mathbf{Q}(\mathbf{U}), \tag{2.5}$$

where the vector of evolved variables $\mathbf{U}$ and the vector of source terms $\mathbf{Q}$ are defined as:

$$\mathbf{U} = \left[\rho_g\alpha_g, \rho_l\alpha_l, \rho_g\alpha_g v_g, \rho_l\alpha_l v_l\right]^{\mathrm{T}}, \tag{2.6}$$

$$\mathbf{Q}(\mathbf{U}) = \left[0, 0, Q_g, Q_l\right]^{\mathrm{T}}, \tag{2.7}$$

and the coefficient matrix $\mathbf{A}$ is defined as in [3]:

$$\mathbf{A}(\mathbf{U}) = \begin{bmatrix} 0 & 0 & 1 & 0 \\ 0 & 0 & 0 & 1 \\ \kappa\left(\rho_l\alpha_g + \Delta p\alpha_l\frac{\partial\rho_l}{\partial p}\right) - v_g^2 & \kappa\left(\rho_g\alpha_g - \Delta p\alpha_g\frac{\partial\rho_g}{\partial p}\right) & 2v_g & 0 \\ \kappa\left(\rho_l\alpha_l - \Delta p\alpha_l\frac{\partial\rho_l}{\partial p}\right) & \kappa\left(\rho_g\alpha_l + \Delta p\alpha_g\frac{\partial\rho_g}{\partial p}\right) - v_l^2 & 0 & 2v_l \end{bmatrix}, \tag{2.8}$$

where κ is defined as:

$$\kappa = \frac{1}{\frac{\partial\rho_g}{\partial p}\alpha_g\rho_l + \frac{\partial\rho_l}{\partial p}\alpha_l\rho_g}, \tag{2.9}$$

and the interface pressure term Δp is defined as:

$$\Delta p = p - p^i = \delta \frac{\alpha_g \alpha_l \rho_g \rho_l}{\rho_g \alpha_l + \rho_l \alpha_g} \left(v_g - v_l\right)^2, \tag{2.10}$$

with $\delta = 1.2$. The interface pressure term Δp ensures that the system remains hyperbolic for physically realistic states. For the cases we consider in this paper the system will always remain hyperbolic, i.e. the coefficient matrix $\mathbf{A}$ will have 4 real and distinct eigenvalues and thus linearly independent eigenvectors. Physically, these eigenvalues correspond to fast pressure waves and slow interface (volume fraction) waves. Although it is possible to derive the analytical expressions for eigenvalues and eigenvectors, these expressions are too complicated to be of practical value. Some useful approximations may be obtained through perturbation techniques [2, 3, 5]:

- *pressure waves:*

$$\lambda^{\mathrm{p}} \approx \frac{\rho_g \alpha_l v_l + \rho_l \alpha_g v_g}{\rho_g \alpha_l + \rho_l \alpha_g} \pm \sqrt{\frac{\rho_g \alpha_l + \rho_l \alpha_g}{\rho_g \alpha_l \partial_p \rho_l + \rho_l \alpha_g \partial_p \rho_g}}, \tag{2.11}$$

- *interface waves:*

$$\lambda^{\mathrm{i}} \approx \frac{\rho_g \alpha_l v_g + \rho_l \alpha_g v_l}{\rho_g \alpha_l + \rho_l \alpha_g} \pm \frac{\sqrt{\Delta p(\rho_g \alpha_l + \rho_l \alpha_g) - \rho_g \rho_l \alpha_g \alpha_l (v_g - v_l)^2}}{\rho_g \alpha_l + \rho_l \alpha_g}. \tag{2.12}$$

These expressions may become inaccurate if the relative velocity becomes too large. In the following, we will not use the approximations (2.11) and (2.12). Instead we will calculate the eigenstructure numerically for increased accuracy.

2.2. Closure relations and thermodynamic submodel

The model is closed by a basic relation between volume fractions and by an equation of state for each phase k:

$$\alpha_g + \alpha_l = 1, \qquad \rho_k = \rho_{k,0} + \frac{p - p_{k,0}}{a_k^2}, \tag{2.13}$$

where the speed of sound a is defined as $a_k^2 = \partial p / \partial \rho_k$. The parameters are $p_{l,0} = 10^5$ Pa, $p_{g,0} = 0$, $\rho_{l,0} = 1000$ kg/m^3, $\rho_{g,0} = 0$, $a_l = 10^3$ m/s and $a_g = \sqrt{10^5}$ m/s. The assumption of equal phase pressures, $p_g = p_l = p$, allows us to write (2.13) in terms of conserved variables:

$$\frac{u_1}{\rho_g(p)} + \frac{u_2}{\rho_l(p)} = 1 \qquad \rightarrow \qquad p = p(u_1, u_2), \tag{2.14}$$

where $u_1 = \rho_g \alpha_g$ and $u_2 = \rho_l \alpha_l$ are elements of the vector of evolved variables $\mathbf{U}$, Eq. (2.6). For details on closure relations and interface pressure modeling we refer to the papers [3, 27].

3. Numerical model

We start by discretizing the homogeneous version of (2.5) by the explicit Euler method in time and a Roe scheme in space:

$$\mathbf{U}_j^{n+1} = \mathbf{U}_j^n - \frac{\Delta t}{\Delta x} \left(\hat{\mathbf{A}}^+_{j-1/2} \Delta \mathbf{U}^n_{j-1/2} + \hat{\mathbf{A}}^-_{j+1/2} \Delta \mathbf{U}^n_{j+1/2} \right), \tag{3.1}$$

where $\mathbf{U}_j^n$ is a discrete approximation of the cell average of $\mathbf{U}$ in the cell with center at x_j and at the time level n, and $\hat{\mathbf{A}}^{\pm}_{j\mp1/2}\Delta\mathbf{U}_{j\mp1/2}$ are flux differences at the cell interfaces $x_{j\mp1/2}$, where we introduce $\Delta\mathbf{U}_{j+1/2} = \mathbf{U}_{j+1} - \mathbf{U}_j$. For more convenient notation, here and throughout the paper, we assume that the absence of a time index implies the time level n.

Herein, the fundamental component is the construction of a Roe matrix $\hat{\mathbf{A}}$, originally proposed for the Euler equations [28]. We are discussing the non-conservative system modeling two-phase flow and we construct the Roe matrix $\hat{\mathbf{A}}$ following the approach found in [5, 3]. Once the Roe matrix $\hat{\mathbf{A}}$ is defined, the positive and negative parts of $\hat{\mathbf{A}}$ are defined through its eigenvalues:

$$\hat{\mathbf{A}}^{\pm} = \hat{\mathbf{R}}\hat{\mathbf{\Lambda}}^{\pm}\hat{\mathbf{R}}^{-1}, \tag{3.2}$$

where $\hat{\mathbf{R}}$ is the matrix of right eigenvectors and $\hat{\mathbf{\Lambda}}$ is the diagonal matrix of eigenvalues with the eigenvalues defined as:

$$\lambda^+ = \max(0, \lambda), \qquad \lambda^- = \min(0, \lambda). \tag{3.3}$$

A known limitation of this scheme is that the time step must satisfy the constraint $C \leq 1$, where C is the Courant number:

$$C = \max_j |\lambda_j| \frac{\Delta t}{\Delta x}. \tag{3.4}$$

In the following, we will describe an extension of the Roe scheme that is not limited by this condition.

3.1. Large Time Step Roe scheme

To extend the standard Roe scheme to the LTS Roe scheme we use the ideas developed by LeVeque [12] and approach used by Lindqvist et al. [22]. We start by recalling that the standard Roe scheme is a three-point scheme:

$$\mathbf{U}_j^{n+1} = \mathbf{U}\left(\mathbf{U}_{j-1}^n, \mathbf{U}_j^n, \mathbf{U}_{j+1}^n\right). \tag{3.5}$$

In the standard Roe scheme this property is ensured by the CFL condition (3.4), which requires that no wave can travel more than one cell during a single time step. As a consequence, the $\mathbf{U}_j^{n+1}$ in the (3.1) is updated only by the flux differences at the cell interfaces $x_{j-1/2}$ and $x_{j+1/2}$, see Figure 1. However, if we increase the time step Δt, the particular wave may travel more than one cell during a single time step. To take this into the account we increase the domain of dependence. Therefore, the value in a particular cell may depend on more than three cells:

$$\mathbf{U}_j^{n+1} = \mathbf{U}\left(..., \mathbf{U}_{j-2}^n, \mathbf{U}_{j-1}^n, \mathbf{U}_j^n, \mathbf{U}_{j+1}^n, \mathbf{U}_{j+2}^n, ...\right), \tag{3.6}$$

where the particular size of the domain of dependence depends on the local Courant number. Since the information from the domain of dependence with which we update cell state $\mathbf{U}_j^{n+1}$ is delivered in terms of flux differences through the cell faces, we reformulate the flux differences to include all flux differences in the domain of dependence. Hence we modify the flux differences in (3.1) to obtain the LTS extension of the Roe scheme:

$$\mathbf{U}_j^{n+1} = \mathbf{U}_j^n - \frac{\Delta t}{\Delta x}\left(\sum_{i=0}^{\infty} \hat{\mathbf{A}}^{i+}_{j-1/2-i}\Delta\mathbf{U}_{j-1/2-i} + \sum_{i=0}^{\infty} \hat{\mathbf{A}}^{i-}_{j+1/2+i}\Delta\mathbf{U}_{j+1/2+i}\right). \tag{3.7}$$

The matrices $\hat{\mathbf{A}}^{i\pm}$ are defined as:

$$\hat{\mathbf{A}}^{i\pm} = \hat{\mathbf{R}}\hat{\mathbf{\Lambda}}^{i\pm}\hat{\mathbf{R}}^{-1}, \tag{3.8}$$

with the eigenvalues defined as in [22]:

$$\lambda^{i\pm} = \pm\max\left(0, \min\left(\pm\lambda - i\frac{\Delta x}{\Delta t}, \frac{\Delta x}{\Delta t}\right)\right). \tag{3.9}$$

The superscripts $i+$ and $i-$ in (3.8) denote the parts of the Roe matrix $\hat{\mathbf{A}}$ defined by the positive ($i+$) and the negative ($i-$) wave speeds λ^{i+} and λ^{i-} at the cell interface located i cells to the left ($i+$) and to the right ($i-$) of the cell interface associated with $i = 0$, i.e. $x_{j+1/2}$. Herein, flux differences associated with $\hat{\mathbf{A}}^{i+}$ and $\hat{\mathbf{A}}^{i-}$ are traveling to the right and left, respectively.

We assume that these flux differences, i.e. the waves they describe are moving independently of each other, i.e. all the interactions between the waves are linear. Figure 1 shows the flux differences that update the cell $\mathbf{U}_j$ in the standard and LTS Roe scheme. We note that even though we allow more waves to pass through the particular interface, the different waves need to travel a different distance before they start "passing" through the relevant interface. This fact is taken into the account by the modification of the eigenvalues in (3.9). Also, we note that the infinite sums in (3.7) will only contain a finite number of nonzero terms, because the term $\lambda - i\frac{\Delta x}{\Delta t}$ becomes negative, and the term $\lambda + i\frac{\Delta x}{\Delta t}$ becomes positive in (3.9) for sufficiently large i. The reader is referred to [22] for a more extensive explanation of the LTS method.

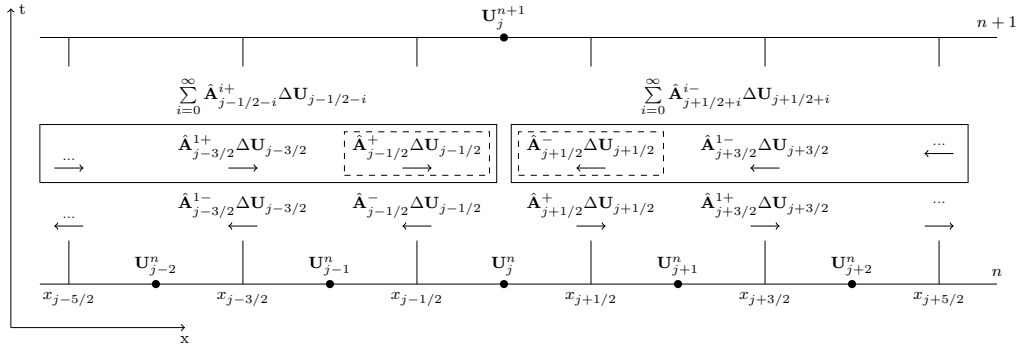

Figure 1: Updating of $\mathbf{U}_j$: domain of dependence and flux differences in standard Roe (dashed boxes) and LTS Roe scheme (full boxes)

4. Boundary conditions

We now discuss how to incorporate boundary conditions into the LTS scheme (3.7). Boundary conditions may be divided into two main categories [14]: *closed*, in which no information is allowed to cross the boundary, and *open*, in which information travels across the boundaries along the waves inherent in the equations, as described for instance in [29].

Herein, the direction of information flow is determined by the sign of the eigenvalues of the matrix $\mathbf{A}$ given by (2.8), with positive eigenvalues corresponding to flow along the positive x-direction. Hence, the number of imposed boundary conditions must correspond to the number of inflowing characteristics at the given boundary.

For the purposes of this paper, we will assume that the flow is subsonic. In that case we have at least one incoming and one outgoing characteristic at each boundary, i.e. one of the pressure

eigenvalues (2.11) will be positive and one will be negative. Then, at each boundary, we are left with 3 different scenarios according to the sign of the interface eigenvalues (2.12):

- No interface eigenvalue represents inflow: 1 boundary condition must be imposed;
- one interface eigenvalue represents inflow: 2 boundary conditions must be imposed;
- both interface eigenvalues represent inflow: 3 boundary conditions must be imposed.

In this paper, we will present a method general enough to handle all these cases. We will however limit ourselves to *constant* boundary conditions, i.e. we consider only cases where both the imposed boundary conditions and the signs of the boundary eigenvalues do not vary in time. This allows us to focus on a main difficulty in the LTS setting (3.7): how to naturally incorporate boundary cells into the increased domain of dependence.

For the first cell in the domain, the standard Roe scheme stencil (3.5) implies:

$$\mathbf{U}_1^{n+1} = \mathbf{U}\left(\mathbf{U}_{\mathrm{LBC}}^n, \mathbf{U}_1^n, \mathbf{U}_2^n\right), \tag{4.1}$$

with $\mathbf{U}_{\mathrm{LBC}}$ being $\mathbf{U}$ in the left boundary cell, where the value at the boundary is typically prescribed for the problem. Clearly, this leads to a difficulty when it comes to the definition of numerical boundary conditions in the LTS method. If we assume that $\mathbf{U}_j$ in (3.6) is the first cell in the domain, then the LTS Roe scheme stencil (3.6) implies:

$$\mathbf{U}_1^{n+1} = \mathbf{U}\left(..., \mathbf{U}_{-1}^n, \mathbf{U}_{\mathrm{LBC}}^n, \mathbf{U}_1^n, \mathbf{U}_2^n, \mathbf{U}_3^n, ...\right). \tag{4.2}$$

Here, we do not have the cell values associated with $\mathbf{U}_{j-1}^n$, $\mathbf{U}_{j-2}^n$, etc. We now suggest two different ways to define these boundary cells.

4.1. Extrapolated boundary conditions

Assume that we apply a Courant number $C > 0$, i.e. we will need $M = \mathrm{ceil}(C)$ numerical ghost cells at each boundary to directly apply the LTS Roe scheme, where $\mathrm{ceil}(C)$ is the smallest integer that is larger or equal to C. The straightforward way to provide these additional cells is to simply extrapolate the values of the original boundary cell. In this way, all additional cells in the boundary zone will have the same values as the original boundary cell:

$$\mathbf{U}_j^n = \mathbf{U}_{\mathrm{LBC}}^n \quad \forall \quad j < \mathrm{LBC}, \tag{4.3}$$

$$\mathbf{U}_j^n = \mathbf{U}_{\mathrm{RBC}}^n \quad \forall \quad j > \mathrm{RBC}, \tag{4.4}$$

where LBC and RBC denote the indices of the left and right boundary cells, respectively. Assuming N cells in the interior domain, we will use the convention that $\mathrm{LBC} = 0$ and $\mathrm{RBC} = N + 1$. We will refer to this formulation as EBC, i.e. extrapolated boundary conditions. If there are no source terms present in the computational domain and the boundary conditions are constant in time this approach will be very effective, and very accurate results may be obtained, as will be shown for the shock tube example.

Next, we are interested how appropriate this definition is when there are source terms present. If we assume constant boundary conditions, the assumption of locally uniform data corresponds to a valid steady state solution in the absence of source terms. Consequently, the application of (4.3) and (4.4) may be viewed as follows:

- Calculate $\mathbf{U}_{\mathrm{LBC}}$ and $\mathbf{U}_{\mathrm{RBC}}$ by some boundary scheme.
- Solve the steady state and homogeneous version of the problem (2.5):

$$\mathbf{A}\,\mathrm{d}_x\mathbf{U} = 0, \tag{4.5}$$

  in an artifical domain extended at the boundaries (the solution is simply $\mathbf{U}$ = const.)
- Transport the solution from this artificial domain into the actual computational domain through the LTS method.

Comparing the steady state form of (2.5) to (4.5), we see that under this point of view the EBC approach assumes there is no effect of the source terms in the boundary cells. Applying a Courant number $C > 1$, we will then see this manifest itself as a discontinuity in the numerical solution, propagating C cells per time step away from the boundary. Clearly, this is a numerical artifact due to the fact that we allow information to travel more than one cell during a single time step, without being affected by the source term. Herein, there are a number of ways of constructing the values of the primary boundary cells at x_{LBC} and x_{RBC}, for instance by extrapolation of the characteristic [30] or primitive variables. However, regardless of our choice of updating $\mathbf{U}_{\mathrm{LBC}}$ and $\mathbf{U}_{\mathrm{RBC}}$, we are left with a central problem associated with the EBC as given by (4.3) and (4.4) in the presence of source terms. We observe that this problem is somewhat independent of the choice of extrapolation variables, and we focus on primitive variable extrapolation for the purposes of this paper.

4.2. Steady state boundary condition

To overcome the problem discussed above, we replace (4.5) by the steady state form of (2.5):

$$\mathbf{A}\,\mathrm{d}_x\mathbf{U} = \mathbf{Q}(\mathbf{U}). \tag{4.6}$$

Assuming that the eigenvalues of $\mathbf{A}$ are nonzero, we obtain:

$$\mathrm{d}_x\mathbf{U} = (\mathbf{A}(\mathbf{U}))^{-1}\,\mathbf{Q}(\mathbf{U}). \tag{4.7}$$

Now, by discretizing this equation at the left and the right boundary cells we obtain the slopes $\delta_x\mathbf{U}_{\mathrm{L}}$ and $\delta_x\mathbf{U}_{\mathrm{R}}$ (left and right, respectively) as:

$$\delta_x\mathbf{U}_{\mathrm{L}} = (\mathbf{A}(\mathbf{U}_{\mathrm{LBC}}))^{-1}\,\mathbf{Q}(\mathbf{U}_{\mathrm{LBC}}), \qquad \delta_x\mathbf{U}_{\mathrm{R}} = (\mathbf{A}(\mathbf{U}_{\mathrm{RBC}}))^{-1}\,\mathbf{Q}(\mathbf{U}_{\mathrm{RBC}}), \tag{4.8}$$

which we then use to formulate the additional boundary cells as:

$$\mathbf{U}_j^n = \mathbf{U}_{\mathrm{LBC}}^n + (j - \mathrm{LBC})\Delta x\delta_x\mathbf{U}_{\mathrm{L}}, \quad \forall \quad j \in [\mathrm{LBC} - M, \ldots, \mathrm{LBC}], \tag{4.9}$$

at the left boundary zone and:

$$\mathbf{U}_j^n = \mathbf{U}_{\mathrm{RBC}}^n + (j - \mathrm{RBC})\Delta x\delta_x\mathbf{U}_{\mathrm{R}}, \quad \forall \quad j \in [\mathrm{RBC}, \ldots, \mathrm{RBC} + M], \tag{4.10}$$

at the right boundary zone. These equations then replace (4.3) and (4.4). We will refer to this formulation as SSBC, i.e. steady state boundary conditions.

Remark 1: *We note that in practice, this approach must be handled with caution. Namely, using* (4.9) *and* (4.10) *may result in negative values of the conserved variables. This will be further addressed in section 5.*

4.3. Numerical example

To illustrate how the presence of a source term causes an error close to the boundary and to show the advantage of using the SSBC we consider a linear advection with a source term:

$$\partial_t u + a\partial_x u = q(u), \qquad a = 1, \tag{4.11}$$

with initial data and source term defined as:

$$u(x, 0) = 1, \qquad q(u) = -0.1u. \tag{4.12}$$

For the problem (4.11) to be well-posed we need a boundary condition at the left boundary. We choose $u(0, t) = 1$. The Eq. (4.11) is solved by the explicit Euler method in time, the LTS upwind scheme in space and an explicit treatment of the source term:

$$u_j^{n+1} = u_j^n - \frac{\Delta t}{\Delta x}\left(\sum_{i=0}^{\infty} a^{i+}_{j-1/2-i}\Delta u_{j-1/2-i} + \sum_{i=0}^{\infty} a^{i-}_{j+1/2+i}\Delta u_{j+1/2+i}\right) + \Delta t q_j(u_j^n), \tag{4.13}$$

where we note that (4.13) is (3.7) applied to the scalar problem (4.11) including the source term. We set $\Delta x = 1$ and evaluate the solution at time $t = 3$. Figure 2a shows the solution obtained with the non–LTS upwind scheme ($\Delta t = 1 \Rightarrow C = 1$, 3 time steps). Next, we consider the solution obtained with the LTS upwind scheme ($\Delta t = 3 \Rightarrow C = 3$, 1 time step) and EBC, see Figure 2b. It can be seen that the EBC approach neglects the effect of the source term during a single LTS step, and then applies the source term only at the end of the LTS step. In addition, the effect of the source term is magnified, since it multiplies Δt and Δt is larger in the LTS method. To fix this issue, we use the SSBC and reconstruct the boundary zone according to (4.6) – (4.10), see Figure 2c.

Here we note that this pattern of error generation in the presence of source term is not limited only to the vicinity of the boundaries. Similar pattern may appear whenever we transport a discontinuity since the LTS method neglects the effect of the source term on the Riemann problem during a single LTS step. In addition, similar mechanism may arise if there are no source terms, but strong nonlinear effects. In that case, the LTS method neglects the nonlinear interactions during a single LTS step, leading to errors that exhibit similar behavior, i.e. transport of sections of constant data unaffected by nonlinear interactions. In section 5 we will discuss errors caused by the source term elsewhere in the domain.

Remark 2: *It should be noted that the discretization* (4.13) *is stable for our illustrative example, but for arbitrary initial data stability may be lost due to interaction between the source and transport terms.*

To demonstrate the performance of the LTS Roe scheme and boundary treatments we consider two test cases. The numerical solutions are obtained by (3.7) and explicit treatment of the source term:

$$\mathbf{U}_j^{n+1} = \mathbf{U}_j - \frac{\Delta t}{\Delta x}\left(\sum_{i=0}^{\infty} \hat{\mathbf{A}}^{i+}_{j-1/2-i}\Delta \mathbf{U}_{j-1/2-i} + \sum_{i=0}^{\infty} \hat{\mathbf{A}}^{i-}_{j+1/2+i}\Delta \mathbf{U}_{j+1/2+i}\right) + \Delta t \mathbf{Q}_j. \tag{4.14}$$

In all the numerical investigations considered below, the time step Δt is fixed and determined at the beginning of the calculation, based on the Courant number we want to use and prior knowledge of the largest eigenvalue that will appear during the computation:

$$\Delta t = \frac{C\Delta x}{\max_{j,n}|\lambda_j^n|}. \tag{4.15}$$

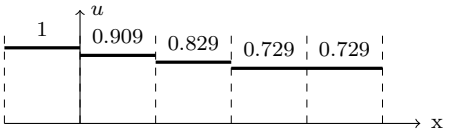

(a) Standard (non–LTS) upwind scheme with $C = 1$

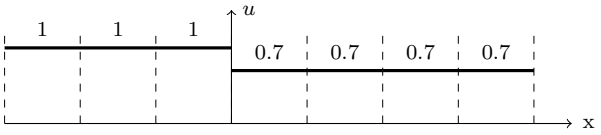

(b) LTS–upwind scheme with $C = 3$ and EBC

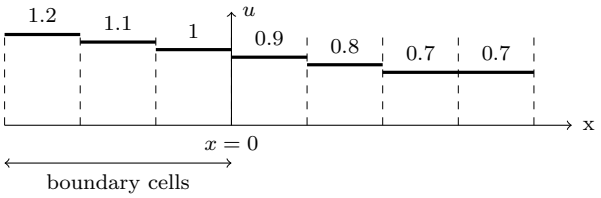

(c) LTS–upwind scheme with $C = 3$ and SSBC

Figure 2: Numerical solution for problem (4.11) after $t = 3$

4.4. Shock tube results

We first consider a shock tube problem studied by Cortes et al. [2] and Evje and Flåtten [3]. The tube has a length of 100 m and initial data with a discontinuity at $x = 50$ m. The initial data on the left and the right of the discontinuity are:

$$\mathbf{V}(x,0) = \left[p, \alpha_l, v_g, v_l\right]^{\mathrm{T}} = \begin{cases} [265000\ \text{Pa}, 0.71, 65\ \text{m/s}, 1\ \text{m/s}] & \text{if } x < 50; \\ [265000\ \text{Pa}, 0.7, 50\ \text{m/s}, 1\ \text{m/s}] & \text{if } x > 50. \end{cases} \tag{4.16}$$

The solution is evaluated at the time $t = 0.1$s. Boundary conditions are obtained by simple extrapolation (EBC), because the waves will not reach the boundaries, therefore no special treatment of the boundaries is required. The numerical solution is obtained with (4.14), and we note that for the shock tube test case $\mathbf{Q}_j^n = 0$. The reference solution is obtained by the Roe scheme with superbee wave limiter on a grid with 12 000 cells and $\Delta t = 2.1815 \cdot 10^{-5}$ s, corresponding to $C \approx 1$.

Figure 3 shows the comparison between the standard and LTS Roe scheme at Courant number $C \approx 5$ and $C \approx 39$ on the grid with 100 cells. It can be seen that the LTS Roe scheme with $C \approx 5$ resolves the left going shock with higher accuracy than non–LTS Roe scheme. The LTS Roe scheme with $C \approx 39$ achieves even higher accuracy. However, one can note that LTS Roe scheme leads to slight overshoots and undershoots which can be best seen in pressure and liquid velocity profiles. Similar oscillations have been observed previously for the Euler equations [22, 18], and are due to the assumption of linear wave interactions. Regardless of these oscillations one should note that the solution obtained with the LTS Roe scheme took only 8 and 1 time steps (ts), respectively, making it more efficient than the standard Roe scheme that took 39 time steps.

We also investigate the convergence of the LTS Roe scheme for different grids and Courant numbers, see Table 1. We can observe that the accuracy increases as we refine the grid and that

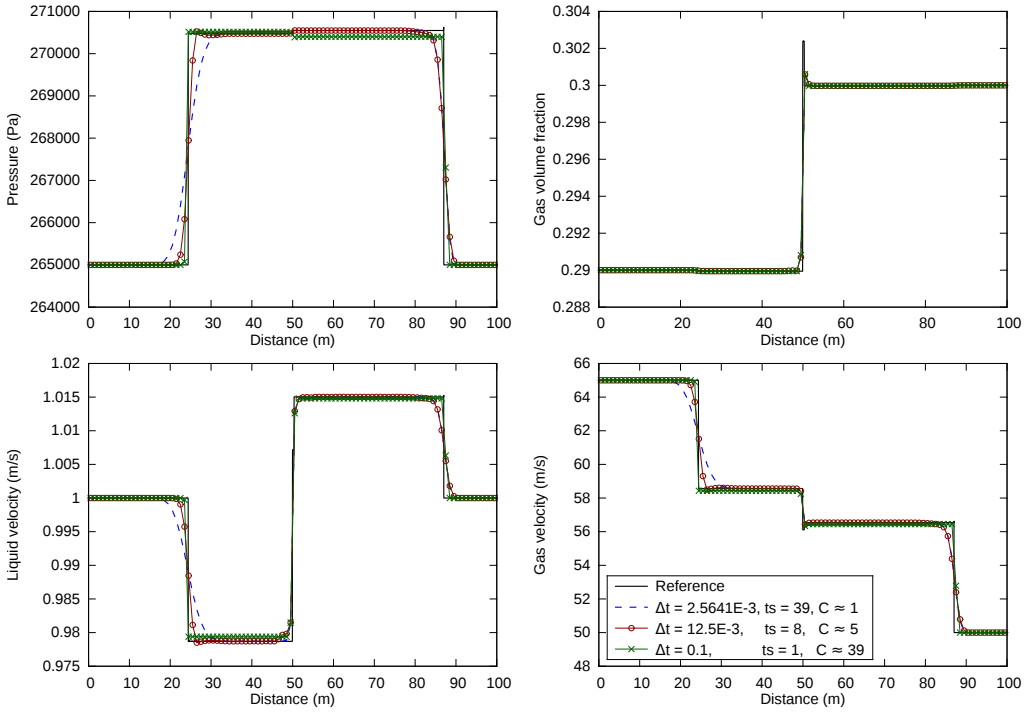

Figure 3: Comparison between standard and LTS Roe scheme on the grid with 100 cells for shock tube problem (4.16)

Table 1: 1-norm error estimate $\mathcal{E}$ ($\times 10^3$ Pa) and convergence rates $\mathcal{L}$ for pressure for shock tube problem (4.16)

	Roe		Roe + superbee		LTS Roe		LTS Roe		LTS Roe	
$\frac{\Delta t}{\Delta x}$	$2.6 \cdot 10^{-3}$ ($C \approx 1$)		$2.6 \cdot 10^{-3}$ ($C \approx 1$)		$1.25 \cdot 10^{-2}$ ($C \approx 5$)		$2.5 \cdot 10^{-2}$ ($C \approx 10$)		0.1 ($C \approx 39$)	
n	$\mathcal{E}_n$	$\mathcal{L}_n$	$\mathcal{E}_n$	$\mathcal{L}_n$	$\mathcal{E}_n$	$\mathcal{L}_n$	$\mathcal{E}_n$	$\mathcal{L}_n$	$\mathcal{E}_n$	$\mathcal{L}_n$
100	15.5	–	4.12	–	8.27	–	6.41	–	11.2	–
200	11.1	0.482	2.58	0.676	6.31	0.390	4.85	0.401	6.54	0.777
400	7.16	0.633	1.04	1.311	4.01	0.654	2.84	0.775	3.25	1.009
800	4.90	0.546	0.52	0.986	2.64	0.605	1.75	0.700	1.59	1.031

in most cases the convergence rate increases as we increase the Courant number. A similar trend is observed for the velocity profiles, while the accuracy and convergence of the volume fraction are somewhat ambiguous due to the presence of the spike, see Figure 3.

4.5. Water faucet results

As a second test case we consider the classical water faucet problem proposed by Ransom [31]. The problem consists of a vertical pipe 12 meters long with initial data:

$$\mathbf{V}(x,0) = \left[p, \alpha_l, v_g, v_l\right]^{\mathrm{T}} = \left[10^5 \text{ Pa}, 0.8, 0 \text{ m/s}, 10 \text{ m/s}\right]. \tag{4.17}$$

The water in the pipe is accelerated due to the effect of gravity which we define as a source term in (2.5):

$$\mathbf{Q}(\mathbf{U}) = [0, 0, g\rho_g\alpha_g, g\rho_l\alpha_l]^{\mathrm{T}}, \tag{4.18}$$

where $g = 9.81$ m/s^2. The solution is computed at time $t = 0.6$ s. In addition, the following boundary conditions are given:

$$\begin{aligned} &\text{Inlet:} \quad \alpha_l = 0.8, \quad v_l = 10 \text{ m/s}, \quad v_g = 0 \text{ m/s}, \\ &\text{Outlet:} \quad p = 10^5 \text{ Pa}. \end{aligned}$$

The remaining values required to determine the evolved variables at the boundary cells are extrapolated from the computational domain, which yields the following set of values at the boundaries:

$$\mathbf{B}^n_{\mathrm{LBC}} = \begin{bmatrix} p \\ \alpha_l \\ v_g \\ v_l \end{bmatrix}^n_{\mathrm{LBC}} = \begin{bmatrix} p^n_1 \\ 0.8 \\ 0 \\ 10 \text{ m/s} \end{bmatrix}, \quad \mathbf{B}^n_{\mathrm{RBC}} = \begin{bmatrix} p \\ \alpha_l \\ v_g \\ v_l \end{bmatrix}^n_{\mathrm{RBC}} = \begin{bmatrix} 10^5 \text{ Pa} \\ (\alpha_l)^n_N \\ (v_g)^n_N \\ (v_l)^n_N \end{bmatrix}. \tag{4.19}$$

The analytical solution for the liquid volume fraction and liquid velocity can be found in [3]. The reference solution for the remaining variables is obtained by the standard Roe scheme with superbee wave limiter on a grid with 12 000 cells and $\Delta t = 2.9154 \cdot 10^{-6}$ s, corresponding to $C \approx 1$.

4.5.1. Effect of time step

Figure 4 shows the comparison between the standard and the LTS Roe scheme with different time steps and different implementations of the boundary conditions on the grid with 100 cells.

It can be seen that the pressure solution obtained with SSBC is smoother and larger than the solution obtained with EBC for corresponding time steps, especially for larger time steps. That is expected regarding smoothness, since the boundaries defined with SSBC introduce a smaller error and provide a smoother transition between the boundary zone and the rest of the domain.

The accuracy of the gas volume fraction and liquid velocity increase as we increase the Courant number. This is because the larger time step Δt leads to a smaller number of time steps, which reduces the numerical diffusion introduced each time we average a cell state, i.e. in each time step. However, the error in the gas velocity near the outlet gets larger for larger Courant numbers. We note that the Courant numbers corresponding to the interface waves are smaller than one for all cases. More rigorous insight into the relation between time step and numerical diffusion can be gained through the modified equation analysis, see for instance Harten et al. [32].

4.5.2. Effect of grid refinement

We also compare the effect of grid refinement starting with a grid of 100 cells and a time step $\Delta t = 0.0017$ s, which corresponds to $C \approx 5$. For each refined grid we keep the Courant number constant, i.e. the ratio $\Delta t/\Delta x = 0.0146 = \text{const.}$, see Figure 5. We again note that the SSBC provides smoother and larger pressure profiles than EBC. However, this effect becomes less significant as the grid is refined. This is expected, since the number of boundary cells remains constant as the total number of grid cells is increased. Hence their relative influence becomes smaller. Nevertheless, practical simulations are often performed on coarse grids due to computational efficiency constraints. Here the results may be sensitive to the different treatments

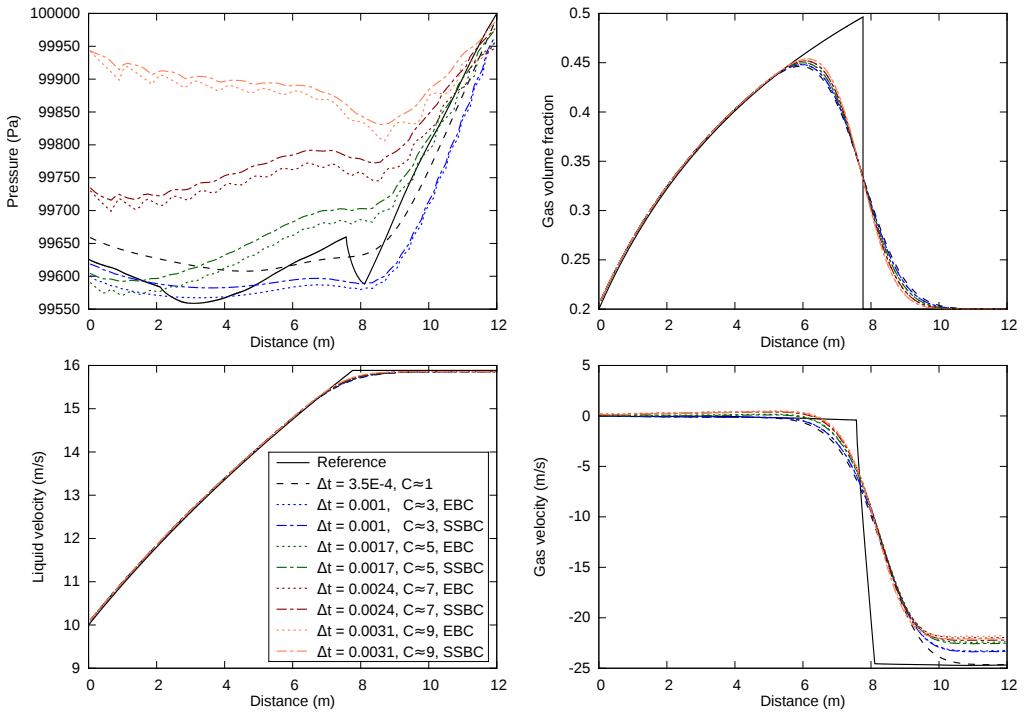

Figure 4: Effect of increasing the time step for different treatments of boundary conditions on the grid with 100 cells for water faucet problem (4.17)

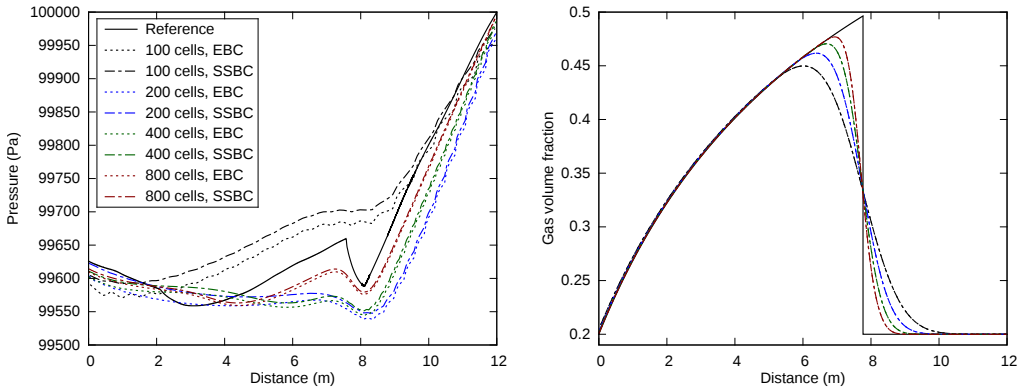

Figure 5: Effect of grid refinement for different treatments of boundary conditions with $\Delta t/\Delta x$ = const., (C $\approx$ 5) for water faucet problem (4.17)

of the boundary conditions presented here. Figure 5 indicates that both with EBC and SSBC, the LTS Roe scheme converges to the exact solution as the grid is refined. A similar trend is observed for the velocities.

To confirm that, we again investigate the convergence of the LTS Roe scheme for different grids and Courant numbers, see Table 2. We can observe that both accuracy and convergence

rate tend to increase as we increase the Courant number and refine the grid. A similar trend is observed for the pressure and velocity profiles.

Table 2: 1-norm error estimate $\mathcal{E}$ ($\times 10^{-2}$) and convergence rates $\mathcal{L}$ for volume fraction for water faucet problem (4.17)

	Roe		Roe + superbee		LTS Roe		LTS Roe		LTS Roe	
$\frac{\Delta t}{\Delta x}$	$2.9 \cdot 10^{-3}$ ($C \approx 1$)		$2.9 \cdot 10^{-3}$ ($C \approx 1$)		$1.46 \cdot 10^{-2}$ ($C \approx 5$)		$2.91 \cdot 10^{-2}$ ($C \approx 10$)		$5.81 \cdot 10^{-2}$ ($C \approx 20$)	
n	$\mathcal{E}_n$	$\mathcal{L}_n$	$\mathcal{E}_n$	$\mathcal{L}_n$	$\mathcal{E}_n$	$\mathcal{L}_n$	$\mathcal{E}_n$	$\mathcal{L}_n$	$\mathcal{E}_n$	$\mathcal{L}_n$
100	20.99	–	1.55	–	18.76	–	15.64	–	7.12	–
200	13.82	0.603	0.85	0.867	12.26	0.614	10.05	0.637	4.01	0.827
400	8.87	0.641	0.50	0.751	7.78	0.655	6.26	0.683	2.10	0.932
800	5.50	0.689	0.28	0.847	4.76	0.707	3.75	0.741	1.10	0.934

5. Source terms

Until now, we applied the explicit Euler method for time integration of the source term $\mathbf{Q}$, cf. Eq. (4.14). That way, the accuracy of solutions for volume fractions and phase velocities were increased at the cost of the accuracy of the pressure profile. The oscillations in the pressure profile did not affect the volume fraction profiles, because interface waves are not strongly affected by the pressure waves, cf. see the results in section 4.5. Further, the pressure waves are not strongly affected by gravity. For the water faucet example this is an acceptable approach as long as we apply the LTS method only to the pressure waves, i.e. the Courant numbers corresponding to interface waves (2.12) are less or equal to one at all times:

$$C^{\mathrm{i}} = \frac{\Delta t}{\Delta x} \max_{j,n} \left| \left(\lambda^{\mathrm{i}}\right)_j^n \right| \leq 1, \tag{5.1}$$

where C^{i} are interface Courant numbers and λ^{i} are the interface eigenvalues (2.12). We note that the eigenvalues associated with the interface waves (2.12) could be further approximated by assuming $\rho_g/\rho_l \approx 0$ for which we would obtain that both interface waves are $\lambda^i \approx v_l$. For the water faucet case considered here this assumption is also justified by numerical investigations.

However, if the source term is discretized with the explicit Euler method, and interface Courant number is increased beyond the standard CFL condition, severe oscillations will appear in the volume fraction and velocity profiles, regardless of how we define additional boundary cells. This suggest that if we want to use the LTS discretization for interface waves we need a more refined treatment of the source term.

In the literature, two improvements to the straightforward Euler discretization of the source term are commonly applied [33]:

- *Operator splitting* [34], which is based on solving the hyperbolic system $\partial_t \mathbf{U} + \mathbf{A}(\mathbf{U})\partial_x \mathbf{U} = 0$ alternately with the ODE $\mathrm{d}\mathbf{U} = \mathbf{Q}(\mathbf{U})$ to approximate the solution to the full problem (2.5).
- *Flux modification* [35], which is based on modifying the numerical flux at the cell interfaces to take into account the effect of the source term during the time step.

LeVeque [36] notes that operator splitting methods may cause difficulties when the system is close to a steady state solution, i.e. when the flux gradients are balanced with the source terms. Schemes that correctly balance the source volume integral with the flux surface integral are

denoted as *well-balanced* schemes, and are most conveniently formulated in the flux modification setting.

In this paper, we will follow the flux modification approach, starting by considering a scalar conservation law. Then, we provide the natural extension to the LTS Roe scheme and the system of equations. We follow the work of Murillo and García-Navarro [23], which again is based on ideas introduced by Bermúdez and Vázquez-Cendón [35]. We will end up formulating a slightly modified discretization.

5.1. Scalar conservation law with source term

We are considering a scalar conservation law with source term in the form:

$$\partial_t u + \partial_x f(u) = q(u), \tag{5.2}$$

with initial data corresponding to the Riemann problem:

$$u(x,0) = \begin{cases} u_\mathrm{L} & \text{if } x < 0; \\ u_\mathrm{R} & \text{if } x > 0. \end{cases} \tag{5.3}$$

We can also write (5.2) in quasilinear form as:

$$\partial_t u + \lambda \partial_x u = q(u), \qquad \lambda = \mathrm{d}_u f(u). \tag{5.4}$$

The Riemann problem (5.3) can be solved exactly by integrating (5.2) over the control volume $[x_\mathrm{L}, x_\mathrm{R}] \times [0, T]$ such that:

$$|\lambda_\mathrm{RP} T| < |x_\mathrm{L}|, |x_\mathrm{R}|, \qquad x_\mathrm{L} < 0 < x_\mathrm{R}, \tag{5.5}$$

where λ_RP is wave speed corresponding to Riemann problem (5.3) determined by the Rankine–Hugoniot condition. By integrating (5.2) in space and time we obtain:

$$\int_{x_\mathrm{L}}^{x_\mathrm{R}} u(x,T)\,\mathrm{d}x = u_\mathrm{R} x_\mathrm{R} - u_\mathrm{L} x_\mathrm{L} + T\left(f(u_\mathrm{L}) - f(u_\mathrm{R})\right) + \int_0^T \int_{x_\mathrm{L}}^{x_\mathrm{R}} q(u)\,\mathrm{d}x\,\mathrm{d}t. \tag{5.6}$$

As a discrete analogue to the above, we consider the local Riemann problem with piecewise initial data:

$$u(x,0) = \begin{cases} u_j & \text{if } x < 0; \\ u_{j+1} & \text{if } x > 0. \end{cases} \tag{5.7}$$

By integrating the local Riemann problem over the corresponding discrete control volume $[-\frac{\Delta x}{2}, \frac{\Delta x}{2}] \times [0, T]$ we obtain:

$$\int_{-\frac{\Delta x}{2}}^{\frac{\Delta x}{2}} u(x,T)\,\mathrm{d}x = \frac{\Delta x}{2}\left(u_{j+1} + u_j\right) + T\left(f(u_j) - f(u_{j+1})\right) + T s_{j+1/2}, \tag{5.8}$$

where we expressed the source term as:

$$T s_{j+1/2} = \int_0^T \int_{x_\mathrm{L}}^{x_\mathrm{R}} q_{j+1/2}\,\mathrm{d}x\,\mathrm{d}t. \tag{5.9}$$

As for now, we will leave the specific ways to evaluate the source term $q_{j+1/2}$ at the interface aside and return to it later, when we consider system of equations, cf. section 5.4. Since we

are considering a scalar conservation law, the Riemann problem (5.7) consists of only one wave traveling either to the right (if $\lambda_{j+1/2} > 0$) or to the left (if $\lambda_{j+1/2} < 0$). If the wave speed $\lambda_{j+1/2}$ is positive, the value of u^+_{j+1} corresponding to the right going wave can be calculated from (5.8) as:

$$\int_{-\frac{\Delta x}{2}}^{0} u(x,T)\,\mathrm{d}x + \int_{0}^{\lambda_{j+1/2}T} u^+(x,T)\,\mathrm{d}x + \int_{\lambda_{j+1/2}T}^{\frac{\Delta x}{2}} u(x,T)\,\mathrm{d}x = \frac{\Delta x}{2}\left(u_{j+1}+u_j\right) + T\left(f(u_j)-f(u_{j+1})\right) + T s_{j+1/2}. \tag{5.10}$$

By using the Rankine–Hugoniot condition:

$$f(u_{j+1}) - f(u_j) = \lambda_{j+1/2}\left(u_{j+1}-u_j\right), \tag{5.11}$$

on the right hand side of (5.10) and the fact that the integrands on the left hand side of (5.10) are equal to u_j, u^+_{j+1} and u_{j+1}, respectively, (5.10) yields:

$$u^+_{j+1} = u_j + \frac{s_{j+1/2}}{\lambda_{j+1/2}}, \tag{5.12}$$

where u^+_{j+1} denotes the state that travels to the right of the Riemann problem, into the cell with center at x_{j+1}. If the wave speed $\lambda_{j+1/2}$ is negative, the corresponding u^-_j is:

$$u^-_j = u_{j+1} - \frac{s_{j+1/2}}{\lambda_{j+1/2}}, \tag{5.13}$$

where u^-_j denotes the state that travels to the left of the Riemann problem, into the cell with center at x_j. Therefore, an arbitrary cell state u_j can be seen as being updated by information from neighboring Riemann problems:

$$u^{n+1}_j \Delta x = u_j \Delta x + (u^+_j - u_j)\lambda^+_{j-1/2}\Delta t - (u^-_j - u_j)\lambda^-_{j+1/2}\Delta t, \tag{5.14}$$

where we recall that $\lambda^\pm$ was defined according to (3.3). By inserting (5.12) and (5.13) into the (5.14) we have:

$$u^{n+1}_j = u^n_j - \frac{\Delta t}{\Delta x}\left(\lambda^+_{j-1/2}\Delta u_{j-1/2} + \lambda^-_{j+1/2}\Delta u_{j+1/2}\right) + \frac{\Delta t}{\Delta x}\left(s^+_{j-1/2} + s^-_{j+1/2}\right), \tag{5.15}$$

with $s^+_{j-1/2}$ and $s^-_{j+1/2}$ defined as:

$$s^+_{j-1/2} = \frac{\lambda^+_{j-1/2}}{\lambda_{j-1/2}} s_{j-1/2}, \qquad s^-_{j+1/2} = \frac{\lambda^-_{j+1/2}}{\lambda_{j+1/2}} s_{j+1/2}. \tag{5.16}$$

We will denote this type of source term discretization as the *split* source discretization, as opposed to *unsplit* explicit Euler discretization. We note that the quotient of eigenvalues in the (5.16) is either zero or one, i.e. the source terms in (5.16) are either zero or $s_{j-1/2}$ or $s_{j+1/2}$, respectively.

Note that, as in the original formulations [35, 23], the expressions (5.16) are not defined if a cell interface eigenvalue is zero. In this case, a convention would be needed to uniquely define the splitting of the source term. As this situation will not arise for any of our test cases, the description (5.16) will be sufficient for our present purposes.

In [23], Murillo and García-Navarro obtain the equivalent of finite volume method (5.15) as:

$$u_j^{n+1} = u_j^n - \frac{\Delta t}{\Delta x}\left(\lambda^+_{j-1/2}\theta_{j-1/2}\Delta u_{j-1/2} + \lambda^-_{j+1/2}\theta_{j+1/2}\Delta u_{j+1/2}\right), \tag{5.17}$$

with $\theta_{j+1/2}$:

$$\theta_{j+1/2} = 1 - \frac{s_{j+1/2}}{\lambda_{j+1/2}(u_{j+1} - u_j)}. \tag{5.18}$$

Although (5.15) and (5.17) are mathematically equivalent, (5.17) suffers from a drawback that source term yields no effect if the initial data is uniform. Since the initial data in the water faucet problem is uniform, it is necessary to use the approach corresponding to (5.15).

Remark 3: *In [23], Murillo and García-Navarro further discuss the effect of source term on the time step Δt and the effect it might have on the positivity preserving property of the scheme. Here, we do not discuss that matter because the water faucet test case, as discussed here, does not contain issues related to loss of positivity.*

5.2. Extension into the LTS framework

In this subsection, we are interested in generalizing this new discretization of the source term into the LTS framework. We start by observing that for a homogeneous problem, (5.15) is the scalar formulation of the flux difference splitting form (3.1). In section 3, the discretization (3.1) was extended into the LTS framework by extending the domain of dependence, i.e. by taking into the account more flux differences, cf. section 3.1. The procedure may be summarized as:

- Take into the account flux difference contributions from all interfaces in the domain of dependence;
- modify the wave speeds associated with flux differences according to (3.9).

By applying these steps, the homogeneous version of (5.15) can be extended into the LTS framework as:

$$u_j^{n+1} = u_j^n - \frac{\Delta t}{\Delta x}\left(\sum_{i=0}^{\infty}\lambda^{i+}_{j-1/2-i}\Delta u_{j-1/2-i} + \sum_{i=0}^{\infty}\lambda^{i-}_{j+1/2+i}\Delta u_{j+1/2+i}\right). \tag{5.19}$$

Based on this, we argue that the same reasoning may be applied on the source term contributions in the (5.15):

- Take into the account source effect contributions from all interfaces in the domain of dependence;
- modify the wave speeds associated with source contribution according to (3.9).

Hence, we obtain the LTS extension of (5.15) as:

$$\begin{aligned} u_j^{n+1} = u_j^n &- \frac{\Delta t}{\Delta x}\left(\sum_{i=0}^{\infty}\lambda^{i+}_{j-1/2-i}\Delta u_{j-1/2-i} + \sum_{i=0}^{\infty}\lambda^{i-}_{j+1/2+i}\Delta u_{j+1/2+i}\right) \\ &+ \frac{\Delta t}{\Delta x}\left(\sum_{i=0}^{\infty}\frac{\lambda^{i+}_{j-1/2-i}}{\lambda_{j-1/2-i}}s_{j-1/2-i} + \sum_{i=0}^{\infty}\frac{\lambda^{i-}_{j+1/2+i}}{\lambda_{j+1/2+i}}s_{j+1/2+i}\right). \end{aligned} \tag{5.20}$$

That way we take into account source effects that are delivered from all interfaces in the domain of dependence, and we ensure that the source terms further away from the cell we are updating contribute less than those closer. We note that in fractions of eigenvalues associated with source terms in (5.20), we modify only the eigenvalue in the numerator. Due to that, the quotient of eigenvalues is not either zero or one anymore, but may gradually decrease from one to zero as we are moving further away from the interface.

5.3. Generalization to system of equations

We are now interested in generalizing (5.20) to systems of equations. We start by generalizing the non-LTS (5.15), and then proceed to generalize (5.20). For homogeneous problem, we already observed that (5.15) is the scalar formulation of the flux difference splitting form (3.1). Hence, we look for the generalization of (5.15) in the form:

$$\mathbf{U}_j^{n+1} = \mathbf{U}_j^n - \frac{\Delta t}{\Delta x}\left(\hat{\mathbf{A}}^+_{j-1/2}\Delta\mathbf{U}_{j-1/2} + \hat{\mathbf{A}}^-_{j+1/2}\Delta\mathbf{U}_{j+1/2}\right) + \frac{\Delta t}{\Delta x}\left(\mathbf{S}^+_{j-1/2} + \mathbf{S}^-_{j+1/2}\right), \tag{5.21}$$

where $\mathbf{S}^{\pm}_{j+1/2}$ will be the system equivalent to $s^{\pm}_{j+1/2}$ in the (5.16). To see how (5.15) generalizes to system of equations, we recall the way the Roe scheme [28] is constructed, but note that for our investigations we consider the Roe matrix $\hat{\mathbf{A}}$ defined for two-fluid model, cf. section 3. We consider the system of equations (2.5) and linearize:

$$\partial_t\mathbf{U} + \hat{\mathbf{A}}_{j+1/2}\partial_x\mathbf{U} = \mathbf{Q}_{j+1/2}, \tag{5.22}$$

where $\mathbf{Q}_{j+1/2}$ is a vector of source terms evaluated at the interface $x_{j+1/2}$. Different ways on how to construct this vector will be addressed in section 5.4. Then, we solve this linearized problem exactly by considering the individual Riemann problem for (5.22) with:

$$\mathbf{U}(x,0) = \begin{cases} \mathbf{U}_j & \text{if } x < 0; \\ \mathbf{U}_{j+1} & \text{if } x > 0. \end{cases} \tag{5.23}$$

We start by multiplying (5.22) by $\hat{\mathbf{R}}^{-1}$, where $\hat{\mathbf{R}}^{-1}$ is the right eigenvector matrix of $\hat{\mathbf{A}} = \hat{\mathbf{A}}_{j+1/2}$:

$$\hat{\mathbf{R}}^{-1}\partial_t\mathbf{U} + \hat{\mathbf{R}}^{-1}\hat{\mathbf{A}}\hat{\mathbf{R}}\hat{\mathbf{R}}^{-1}\partial_x\mathbf{U} = \hat{\mathbf{R}}^{-1}\mathbf{Q}_{j+1/2}, \tag{5.24}$$

to obtain:

$$\partial_t\mathbf{W} + \hat{\mathbf{\Lambda}}\partial_x\mathbf{W} = \mathbf{\Omega}_{j+1/2}, \tag{5.25}$$

where $\mathbf{W} = \hat{\mathbf{R}}^{-1}\mathbf{U}$ is the vector of characteristic variables, $\hat{\mathbf{\Lambda}}$ is the diagonal matrix of eigenvalues, and $\mathbf{\Omega}_{j+1/2} = \hat{\mathbf{R}}^{-1}\mathbf{Q}_{j+1/2}$ is the vector of characteristic source terms. This way we decoupled the system (5.22) into linear advection equations. Then we solve each of these equations according to the theory we presented for scalar conservation laws, section 5.1. Therefore, for each characteristic variable w^p of vector $\mathbf{W}$ we have equation equivalent to (5.15):

$$\begin{aligned}(w^p)_j^{n+1} = (w^p)_j^n &- \frac{\Delta t}{\Delta x}\left((\lambda^p)^+_{j-1/2}\Delta w^p_{j-1/2} + (\lambda^p)^-_{j+1/2}\Delta w^p_{j+1/2}\right) \\ &+ \frac{\Delta t}{\Delta x}\left((s^p)^+_{j-1/2} + (s^p)^-_{j+1/2}\right) \quad \forall p,\end{aligned} \tag{5.26}$$

where s^p is p-th component of vector $\mathbf{S}$. We note that $\mathbf{S}$ is obtained by integrating components of $\mathbf{\Omega}$ as done with $q_{j+1/2}$ in (5.9):

$$T\mathbf{S}_{j+1/2} = \int_0^T \int_{x_\mathrm{L}}^{x_\mathrm{R}} \mathbf{\Omega}_{j+1/2}\,\mathrm{d}x\,\mathrm{d}t. \tag{5.27}$$

Following LeVeque [36], the flux difference terms in Eq. (3.1) may be defined as:

$$\hat{\mathbf{A}}^{\pm}\Delta\mathbf{U}_{j+1/2} = \hat{\mathbf{R}}\hat{\mathbf{\Lambda}}^{\pm}\hat{\mathbf{R}}^{-1}\Delta\mathbf{U}_{j+1/2} = \sum_{p=1}^{m} (\lambda^p)^{\pm}\, r^p \Delta w^p_{j+1/2}. \tag{5.28}$$

Similarly, we argue that the *split* source term can be defined as:

$$\mathbf{S}^{\pm}_{j+1/2} = \hat{\mathbf{R}}\hat{\mathbf{\Lambda}}^{\pm}\hat{\mathbf{\Lambda}}^{-1}\hat{\mathbf{R}}^{-1}\mathbf{S}_{j+1/2} = \sum_{p=1}^{m} \frac{(\lambda^p)^{\pm}}{\lambda^p} r^p s^p_{j+1/2}. \tag{5.29}$$

Therefore we have that:

$$\mathbf{S}^{\pm}_{j+1/2} = \tilde{\mathbf{A}}^{\pm}_{j+1/2}\mathbf{S}_{j+1/2}, \tag{5.30}$$

where we introduced:

$$\tilde{\mathbf{A}}^{\pm} = \hat{\mathbf{R}}\tilde{\mathbf{\Lambda}}^{\pm}\hat{\mathbf{R}}^{-1}, \tag{5.31}$$

$$\tilde{\mathbf{\Lambda}}^{\pm} = \hat{\mathbf{\Lambda}}^{\pm}\hat{\mathbf{\Lambda}}^{-1}. \tag{5.32}$$

Here we point out that (5.30) is system equivalent of (5.16), where term $\tilde{\mathbf{A}}^{\pm}_{j+1/2}$ in (5.30) corresponds to the quotients of eigenvalues in (5.16). Here, just as in the (5.16), the diagonal elements of matrix $\tilde{\mathbf{\Lambda}}^{\pm}$ in (5.32) take the values of either zero or one.

Once we have established the relation between (5.15) and (5.21), we are left with the task of establishing the LTS framework for (5.21). Recall that in section 3 we extended (3.1) to the LTS framework (3.7) by extending the domain of dependence. The same idea was applied in extending the scalar conservation law with source term (5.15) to the LTS framework (5.20). Following that idea, we propose the LTS discretization of the source terms (5.30) in Eq. (5.21) as:

$$\mathbf{S}^{+}_{j+1/2} = \tilde{\mathbf{A}}^{+}_{j+1/2}\mathbf{S}_{j+1/2} \longrightarrow \sum_{i=0}^{\infty} \tilde{\mathbf{A}}^{i+}_{j+1/2-i}\mathbf{S}_{j+1/2-i}, \tag{5.33}$$

$$\mathbf{S}^{-}_{j+1/2} = \tilde{\mathbf{A}}^{-}_{j+1/2}\mathbf{S}_{j+1/2} \longrightarrow \sum_{i=0}^{\infty} \tilde{\mathbf{A}}^{i-}_{j+1/2+i}\mathbf{S}_{j+1/2+i}, \tag{5.34}$$

with:

$$\tilde{\mathbf{A}}^{i\pm} = \hat{\mathbf{R}}\tilde{\mathbf{\Lambda}}^{i\pm}\hat{\mathbf{R}}^{-1}, \tag{5.35}$$

$$\tilde{\mathbf{\Lambda}}^{i\pm} = \hat{\mathbf{\Lambda}}^{i\pm}\hat{\mathbf{\Lambda}}^{-1}. \tag{5.36}$$

The modification of eigenvalues in (5.36) has the same role as with the flux difference contributions – source terms coming from interfaces further away from relevant interface are contributing less than the source terms closer to the relevant interface, due to the fact that they have to travel a certain distance before they start passing through the relevant interface. Here, we note that the diagonal elements of matrix $\tilde{\mathbf{\Lambda}}^{i\pm}$ in (5.36) are not either zero or one, respectively, but may instead gradually decrease towards zero.

5.4. On the choice of average for $\mathbf{Q}_{j+1/2}$

Herein we propose two different ways on how to approximate the source term $\mathbf{Q}_{j+1/2}$ in (5.22) at the cell interface. As a first choice we propose the arithmetic average of $\mathbf{Q}$ in neighboring cells, i.e. a *central* discretization:

$$\mathbf{Q}_{j+1/2} = \frac{1}{2}\left(\mathbf{Q}_j + \mathbf{Q}_{j+1}\right). \tag{5.37}$$

An alternative choice is to take into the account the physics of the particular problem. This may be done by considering the signs of the eigenvalues and defining:

$$\mathbf{Q}_{j+1/2} = \tilde{\mathbf{A}}^{-}_{j+1/2}\mathbf{Q}_j + \tilde{\mathbf{A}}^{+}_{j+1/2}\mathbf{Q}_{j+1}, \tag{5.38}$$

which will be denoted as *upwind* discretization of the source term. We note that $\tilde{\mathbf{A}}^{\pm}_{j+1/2}$ was defined in (5.31).

5.5. Water faucet results

Herein, we once again consider the water faucet test case from section 4.5 and use the same initial data, boundary conditions and means of obtaining the reference solution.

In this section we are interested in increasing the global Courant number so that even the interface Courant number (5.1) exceeds the standard CFL limit. Table 3 shows several global Courant numbers estimated on prior knowledge of the largest wave speeds and the corresponding largest interface Courant numbers C^{i} at starting and end time.

Table 3: Global Courant numbers C with time steps Δt and largest interface Courant number C^{i} on grid with 100 cells

Global C	Δt in s	C^{i} ($t = 0$)	C^{i} ($t = 0.6$ s)
≈ 1	3.4985×10^{-4}	0.030	0.049
≈ 10	0.0035	0.300	0.490
≈ 30	0.0103	0.879	1.444
≈ 49	0.0171	1.459	2.398

5.5.1. Treatment of boundary conditions for very large Courant numbers

At the moment, it remains ambiguous what is the optimal way to apply SSBC approach (cf. section 4) when we use very large Courant numbers. Namely, we wish to apply SSBC to as many boundary cells as possible to reduce the oscillations in the pressure. At the same time, applying (4.9) and (4.10) directly may lead to negative values of the conserved variables. We observed that if interface Courant number (5.1) is higher than one, using EBC will lead to oscillations in volume fraction as well. The error will develop in a similar manner as the error in the pressure profile discussed in section 4, i.e. there will be a step-like pattern in the volume fraction profile. Since in this section we are interested in volume fraction profiles we apply SSBC to just enough cells to ensure that we apply the SSBC to the interface waves. Regardless of how we define the remaining cells, their treatment will affect only the pressure waves and at the moment these waves are not the focus of our interest. Therefore, we used:

- Left boundary: by examining the Table 3 and noting that the domain of dependence of interface waves consists of at most three upwind cells, we used the SSBC approach for five boundary cells at the left boundary.

- Right boundary: at the right boundary we applied SSBC on all the boundary cells because it did not cause any of the conserved variables to become negative.

A more rigorous and more general framework on how to properly apply SSBC in the LTS Roe scheme is being currently investigated.

Remark 4: *As discussed above, using EBC when the interface Courant number is larger than one leads to a step-like error in the volume fraction. We found that this error is independent of how we treat the source term, i.e. it yields the same error for both unsplit and split discretization of the source term and it is not affected by the choice of average for* $\mathbf{Q}_{j+1/2}$. *This justifies our simplification to treat errors caused by the source terms in the vicinity of the boundaries and the errors caused by the treatment of source terms elsewhere in the domain as independent problems.*

5.5.2. Comparison between different discretizations of source term at Courant number $C \approx 30$

Figure 6 shows the comparison of results for the water faucet problem solved by standard Roe scheme, standard Roe scheme with superbee limiter and three different discretizations of the source term for global Courant number $C \approx 30$, all on the grid with 100 cells. The pressure

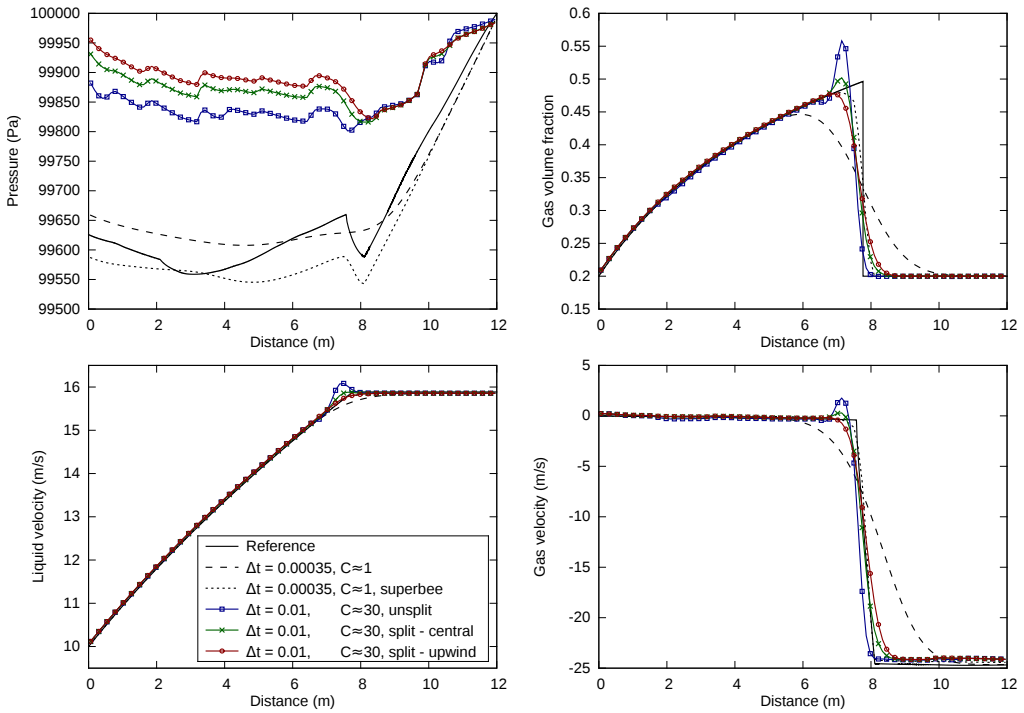

Figure 6: Effect of source term treatment at $C = 30$ on grid with 100 cells for for water faucet problem (4.17)

profiles associated with the LTS method show strong oscillations which are due to the very large global Courant number and somewhat ambiguous treatment of boundary conditions that may affect the accuracy of the pressure waves, see section 5.5.1. In addition, these pressure profiles seem to stabilize themselves at a values slightly lower than the prescribed outlet pressure (10^5 Pa). Regardless of that, the volume fraction waves were not affected by the oscillations of the pressure, and therefore we do not focus on these errors.

In the plot for the volume fraction, we may see that the standard *unsplit* treatment leads to a very large error in the volume fraction on the upstream side of the contact discontinuity, while the corresponding *split* discretizations yield much better solution. The best solution is obtained by using the *upwind* approximation for the source term (5.38). This hierarchy is expected, and may be explained in a following way. First, we note that the error manifests itself as an increase in gas volume fraction. Second, we recall that the source term in (2.5) and the corresponding discretization in (5.21) are positive. The source term is given by the (4.18), where gravity g is constant, while the changes in volume fractions dominate the changes in densities. When we update cell $\mathbf{U}_j$, and we treat the source term with *unsplit* approach, we simply multiply the strength of the source term at that cell by time step Δt. We may observe that this is not true, because what actually enters the cell is coming from the upstream direction, and upstream of the contact discontinuity the volume fraction is smaller than in the cell at x_j. Hence, this approach overestimates the amount of gas phase. Following the same reasoning, we may see why central discretization yields a better solution. The central discretization (5.37) of the split source term uses the volume fractions, i.e. the source terms from upstream interfaces, where value at each interface is determined according to (5.37). This approach uses smaller values of volume fraction, and these values give much better results, but they still overestimate the source strength in the cell at x_j. Upwind discretization (5.38) uses even smaller values of the volume fraction than the central discretization, and does not lead to too large accumulation of the volume fraction in the cell at x_j. We may observe that the accuracy of the best solution obtained with the LTS Roe scheme is much closer to the high resolution Roe scheme than to the standard Roe scheme.

The same hierarchy of the solutions is observed for the liquid and gas velocity profiles. We note that for the gas velocity profile all LTS Roe schemes results seem to stabilize around a slightly too big outlet velocity at the right boundary.

5.5.3. Comparison between different discretizations of source term at Courant number $C \approx 49$

Next we further increase the Courant number and compare different choices of average for $\mathbf{Q}_{j+1/2}$ with *split* discretization of the source term, Figure 7.

For Courant number $C \approx 49$ the accuracy of pressure profiles is further decreased. In addition, the pressure profiles corresponding to Courant number $C \approx 49$ stabilize themselves at different values than before, but still not at the prescribed outlet pressure (10^5 Pa). Once again, we do not focus on these errors, because we concluded that they do not significantly affect the volume fractions and the velocity profiles.

For the volume fractions, further increase of the Courant number leads to further increase in the error upstream of the contact discontinuity. At $C \approx 49$, only the *split* discretization of the source term with upwind average for $\mathbf{Q}_{j+1/2}$ gives reasonably good solutions, although if we further increase the Courant number or the simulation time this error keeps increasing. Similar trend is observed for the velocities. Therefore, even though our new approach significantly improves the solution compared to the explicit treatment of the source term, it does not guarantee an unconditionally stable treatment of the source term.

Remark 5: *Herein, we note that the error in the volume fraction upstream of the contact discontinuity is independent of the way we treat boundary conditions, i.e. it is the same for the EBC and SSBC. This is in agreement with remark 4.*

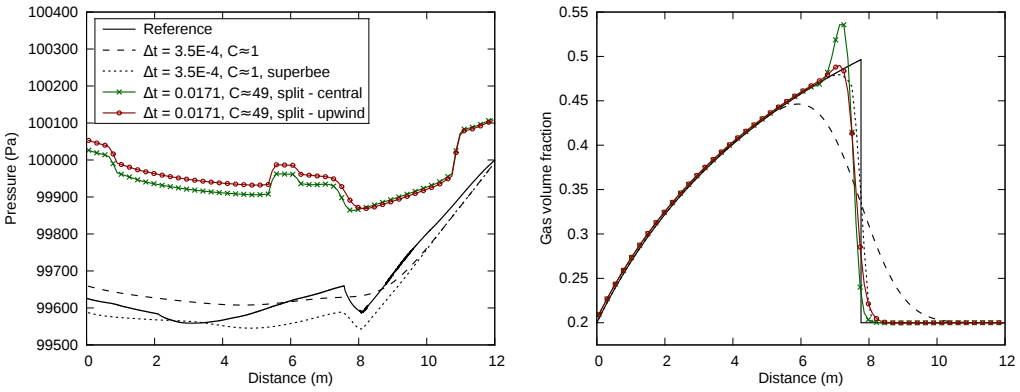

Figure 7: Effect of source term treatment at $C = 49$ on grid with 100 cells for for water faucet problem (4.17)

6. Computational performance

Through the paper, it was repeatedly stated that the LTS Roe scheme is more efficient than the standard Roe scheme. Herein, we investigate the computational efficiency of the LTS Roe scheme by examining the relationship between the computational time and the 1-norm of the error for different grids and Courant numbers, Fig. 8.

For the shock tube problem (4.16) (Fig. 8a) we used the EBC treatment of the boundary conditions. For the water faucet problem (4.17) (Fig. 8b) we used the SSBC treatment of the boundary conditions as described in section 5.5.1 and upwind treatment of the source term with the average (5.38). The CPU times are obtained with the MATLAB tic–toc function averaged over several simulations. We observe that:

- For all the cases, the LTS Roe scheme is more accurate than the standard Roe scheme;
- at each grid size, the increase of Courant number leads to an increase of the efficiency;
- for the shock tube problem (4.16) (Fig. 8a) the optimal Courant number depends on the grid size. The convergence rate indicates that as we refine the grid, the solution obtained with the highest Courant number will achieve the highest accuracy.

We note that these results are dependent on numerical implementation of the method and the features of the studied problems. However, similar results were independently obtained by Lindqvist and Lund [21].

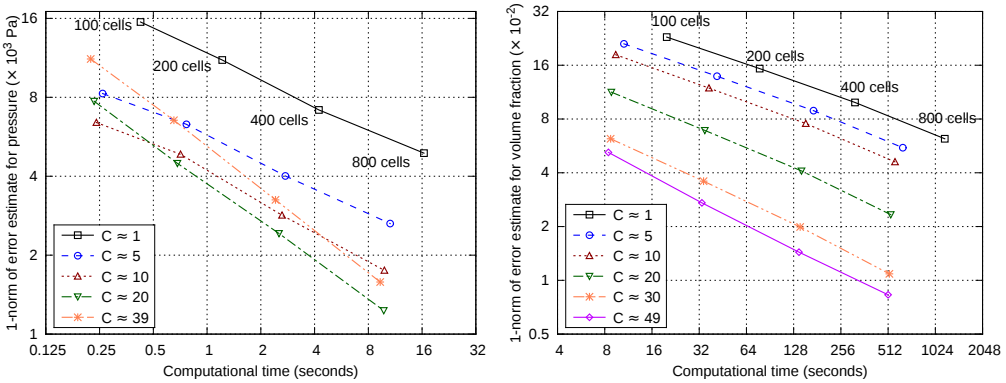

(a) Shock tube problem (4.16) (b) Water faucet problem (4.17)

Figure 8: 1–norm error estimate $\mathcal{E}$ vs. computational time on grids with 100, 200, 400 and 800 cells

7. Conclusions

We extended the standard Roe scheme to the LTS Roe scheme and showed that the two-fluid model can be solved with an explicit method not limited by the CFL condition. We applied the LTS Roe scheme to two test cases, shock tube and water faucet, and focused on the difficulties related to the treatment of boundary conditions and source terms.

The LTS Roe scheme performed very well for the shock tube test case, where there are neither source terms nor difficulties associated with boundary conditions. For the water faucet test case, applying the LTS Roe scheme with the most simple treatment of boundary conditions and source terms led to two distinct, but related, patterns of error generation. The first error is associated with the effect of the source term in the vicinity of the boundary. It is highly dependent on the definition of the boundary cells, and it was shown that this error can be reduced by imposing the steady state boundary conditions (SSBC). In particular, the SSBC approach reduced the oscillations and led to smoother profiles of all variables affected by this error. The second error is associated with the effect of the source term in general, and it is highly dependent on the discretization of the source term. This error was especially important when the interface Courant numbers were increased above one, since it caused severe oscillations in the volume fractions and velocities. It was shown that an appropriate *split* discretization of the source term allows us to use interface Courant numbers up to up to $C^{\mathrm{i}} \approx 2.4$, which corresponds to global Courant number $C \approx 49$. However, the oscillations associated with the pressure profile remained, and got even worse as we increased the Courant number. Reducing the oscillations caused by the source term in the vicinity of the boundaries by introducing SSBC treatment of the boundary conditions and reducing the oscillations in volume fractions and velocities caused by the source term elsewhere in the domain by introducing the *split* discretization of the source term are the main contributions of this paper.

Finally, it was shown that the LTS Roe scheme is more efficient than the standard Roe scheme for all the cases investigated in this paper. Further, the convergence analysis suggests that increasing the Courant number increases the convergence rate. The optimal choice of the Courant number remains to be determined for each particular problem.

The proposed method shows promising potential, especially in the following cases. First, for the problems where there are no source terms and where complex wave dynamics is not

happening close at the boundaries. Second, in problems with a large number of grid cells where the number of additional ghost cells introduced by the LTS method is relatively small compared to the number of grid cells in the domain. And last, in problems where the velocities of the phases are much smaller than the pressure wave speeds and we are not interested in maximum accuracy of the pressure field compared to the accuracy required for volume fractions and velocities.

We believe that the interface Courant number can be further increased by more appropriate treatment of the source term. First, errors observed in Figure 6 led to an erroneous overshoots in velocities, and for our investigations we used fixed time step determined at the beginning of the simulation. Hence, adaptive time stepping procedure may be more appropriate for situations when the LTS method may cause overshoots in velocity. Second, the *split* discretization of the source term, although more successful than standard discretization of the source term, does not take into the account effect of the source term during single LTS steps. These effects may be taken into consideration by investigating the discretization of the source term in direction of well-balanced schemes or some completely new approach, for example by taking into the account the modification of the wave speeds by the source term. As for now, these investigations remain outside the scope of this paper.

Acknowledgments

This paper is an extension of a conference paper [37] that was presented at the Eleventh International Conference on CFD in the Minerals and Process Industries (CFD2015), and was nominated for invitation into the CFD2015 Special Issue of Applied Mathematical Modelling based on its designation as a high-quality paper of relevance to the modelling of fluids-based systems.

The authors were supported by the Research Council of Norway (234126/30) through the SIMCOFLOW project. We are grateful to our colleagues Sigbjørn Løland Bore, Stein Tore Johansen, Ernst Meese and Marica Pelanti for fruitful discussions.

References

[1] J. Cortes, On the construction of upwind schemes for non-equilibrium transient two-phase flows, Comput. Fluids 31 (2) (2002) 159–182.

[2] J. Cortes, A. Debussche, I. Tuomi, A Density Perturbation Method to Study the Eigenstructure of Two-Phase Flow Equation Systems, J. Comput. Phys. 147 (2) (1998) 463–484.

[3] S. Evje, T. Flåtten, Hybrid flux-splitting schemes for a common two-fluid model, J. Comput. Phys. 192 (1) (2003) 175–210.

[4] S. T. Munkejord, Comparison of Roe-type methods for solving the two-fluid model with and without pressure relaxation, Comput. Fluids 36 (6) (2007) 1061–1080.

[5] I. Toumi, A. Kumbaro, An Approximate Linearized Riemann Solver for a Two-Fluid Model, J. Comput. Phys. 124 (2) (1996) 286–300.

[6] F. De Vuyst, Stable and accurate hybrid finite volume methods based on pure convexity arguments for hyperbolic systems of conservation law, J. Comput. Phys. 193 (2) (2004) 426–468.

[7] M. Larsen, E. Hustvedt, P. Hedne, T. Straume, PeTra: A Novel Computer Code for Simulation of Slug Flow, in: SPE Annual Technical Conference and Exhibition, 5-8 October, San Antonio, Texas, Society of Petroleum Engineers, 1997, SPE 38841.

[8] K. Bendiksen, D. Maines, R. Moe, S. Nuland, The Dynamic Two-Fluid Model OLGA: Theory and Application, SPE Prod. Eng. 6 (2) (1991) 171–180.

[9] F. Barre, M. Bernard, The CATHARE code strategy and assessment, Nucl. Eng. Des. 124 (3) (1990) 257–284.

[10] R. J. LeVeque, Large Time Step Shock-Capturing Techniques for Scalar Conservation Laws, SIAM J. Numer. Anal. 19 (6) (1982) 1091–1109.

[11] R. J. LeVeque, Convergence of a Large Time Step Generalization of Godunov's Method for Conservation Laws, Comm. Pure Appl. Math. 37 (4) (1984) 463–477.
[12] R. J. LeVeque, A large Time Step Generalization of Godunov's Method for Systems of Conservation Laws, SIAM J. Numer. Anal. 22 (6) (1985) 1051–1073.
[13] J. Murillo, P. García-Navarro, P. Brufau, J. Burguete, Extension of an explicit finite volume method to large time steps (CFL>1): application to shallow water flows, Int. J. Numer. Meth. Fluids 50 (1) (2006) 63–102.
[14] M. Morales-Hernández, P. García-Navarro, J. Murillo, A large time step 1D upwind explicit scheme (CFL>1): Application to shallow water equations, J. Comput. Phys. 231 (19) (2012) 6532–6557.
[15] M. Morales-Hernández, J. Murillo, P. García-Navarro, J. Burguete, A large time step upwind scheme for the shallow water equations with source terms, in: E. Vázquez Cendón, A. Hidalgo, P. García-Navarro, L. Cea (Eds.), Numerical Methods for Hyperbolic Equations, CRC Press, 2012, pp. 141–148.
[16] M. Morales-Hernández, M. Hubbard, P. García-Navarro, A 2D extension of a Large Time Step explicit scheme (CFL>1) for unsteady problems with wet/dry boundaries, J. Comput. Phys. 263 (2014) 303–327.
[17] R. Xu, D. Zhong, B. Wu, X. Fu, R. Miao, A large time step Godunov scheme for free-surface shallow water equations, Chinese Sci. Bull. 59 (21) (2014) 2534–2540.
[18] Z. Qian, C.-H. Lee, A class of large time step Godunov schemes for hyperbolic conservation laws and applications, J. Comput. Phys. 230 (19) (2011) 7418–7440.
[19] K. Tang, A. Beccantini, C. Corre, Combining Discrete Equations Method and upwind downwind-controlled splitting for non-reacting and reacting two-fluid computations: One dimensional case, Comput. Fluids 93.
[20] N. N. Makawana, A. Chatterjee, Fast Solution of Time Domain Maxwell's Equations Using Large Time Steps, in: 2015 IEEE International Conference on Computational Electromagnetics (ICCEM), 2-5 February, Hong Kong, Institute of Electrical and Electronics Engineers (IEEE), 2015, pp. 330–332.
[21] S. Lindqvist, H. Lund, A Large Time Step Roe scheme scheme applied to two-phase flow, in: M. Papadrakakis, V. Papadopoulos, G. Stefanou, V. Pleveris (Eds.), VII European Congress on Computational Methods in Applied Sciences and Engineering, 5-10 June, Crete Island, Greece, 2016.
[22] S. Lindqvist, P. Aursand, T. Flåtten, A. Solberg, Large Time Step TVD schemes for Hyperbolic Conservation Laws, SIAM J. Numer. Anal. 54 (5) (2016) 2775–2798.
[23] J. Murillo, P. García-Navarro, Weak solutions for partial differential equations with source terms: Application to the shallow water equations, J. Comput. Phys. 229 (11) (2010) 4327–4368.
[24] H. Städtke, Gasdynamic Aspects of Two-Phase Flow, Wiley-VCH, 2006.
[25] H. Holmås, T. Sira, M. Nordsveen, H. P. Langtangen, R. Schulkes, Analysis of a 1D incompressible two-fluid model including artificial diffusion, IMA J. Appl. Math. 73 (4) (2008) 651–667.
[26] A. A. Solberg, Large Time Step explicit schemes for partial differential evolution equations, Master's thesis, Dept. of Energy and Process Engineering, Norwegian University of Science and Technology (2016).
URL `http://hdl.handle.net/11250/2409951`
[27] T. Flåtten, A. Morin, On interface transfer terms in two-fluid models, Int. J. Multiph. Flow 45 (2012) 24–29.
[28] P. Roe, Approximate Riemann solvers, parameter vectors, and difference schemes, J. Comput. Phys. 43 (2) (1981) 357–372.
[29] S. T. Munkejord, Partially-reflection boundary conditions for transient two-phase flow, Commun. Numer. Meth. Engng. 22.
[30] K. Fjelde, K. Karlsen, High-resolution hybrid primitive-conservative upwind schemes for the drift flux model, Comput. Fluids 31 (3) (2002) 335–367.
[31] V. Ransom, Numerical benchmark tests, Multiphase Sci. Tech. 3 (1–4) (1987) 465–473.
[32] A. Harten, J. M. Hyman, P. D. Lax, B. Keyfitz, On Finite-Difference Approximations and Entropy Conditions for Shocks, Comm. Pure Appl. Math. 29 (3) (1976) 297–322.
[33] H. Lund, F. Müller, B. Müller, P. Jenny, Rankine–Hugoniot–Riemann solver for steady multidimensional conservation laws with source terms, Comput. Fluids 101 (2014) 1–14.
[34] R. J. LeVeque, Balancing Source Terms and Flux Gradients in High-Resolution Godunov Methods: The Quasi-Steady Wave-Propagation Algorithm, J. Comput. Phys. 146 (1) (1998) 346–365.
[35] A. Bermúdez, M. E. Vázquez-Cendón, Upwind methods for hyperbolic conservation laws with source terms, Comput. Fluids 23 (8) (1994) 1049–1071.
[36] R. J. LeVeque, Finite Volume Methods for Hyperbolic Problems, Cambridge University Press, 2002.
[37] M. Prebeg, T. Flåtten, B. Müller, Boundary and source term treatment in the Large Time Step method for a common two-fluid model, in: C. B. Solnordal, P. Liovic, G. W. Delaney, S. J. Cummins, M. P. Schwarz, P. Witt (Eds.), The 11th International Conference on CFD in the Minerals and Process Industries, 7-9 December, Melbourne, Australia, 2015.